JACS Au
AN OPEN ACCESS JOURNAL OF THE AMERICAN CHEMICAL SOCIETY

pubs.acs.org/jacsau
Article

From Batch to Continuous Operation: Hydrogenation of Bicarbonate to Formate at Multiphase Boundaries in a Continuous Stirred-Tank Reactor

Mariko Inoue,[#] Gul Afreen,[#] Kazuhito Wada, Matteo Tafuro, Kodai Nogami, Evgeny A. Uslamin, Atul Bansode, Hideaki Tsuneki, Makoto Hirano,* and Atsushi Urakawa*

Cite This: JACS Au 2026, 6, 3386−3393
Read Online

ACCESS | Metrics & More | Article Recommendations | Supporting Information

ABSTRACT: The utilization of carbon dioxide (CO_2) as a C_1 building block has emerged as a promising strategy for sustainable chemical production. Among various CO_2-derived products, formate and formic acid are particularly attractive due to their roles as hydrogen carriers, fuel cell feedstocks, and industrial intermediates. Recent advances in Ru-based homogeneous catalysis have enabled efficient hydrogenation of bicarbonate, which was prepared from CO_2, in biphasic and triphasic systems. In this study, we employed a continuous stirred-tank reactor (CSTR) for the triphasic hydrogenation of $KHCO_3$ under high-pressure conditions (50 bar of H_2), and optimized the stirring conditions using a view cell to ensure efficient mixing. A kinetic model assuming a slow-reaction regime and incorporating the reverse reaction was developed, which accurately predicted the residence time−yield relationship and enabled high formate yields through residence-time optimization. Furthermore, the addition of tris(2,4-di-*tert*-butylphenyl)phosphite as an antioxidant effectively suppressed residual oxygen contamination, which is a known challenge in flow systems. Catalyst recycling and phase separation were successfully integrated into the flow setup, demonstrating the practicality and scalability of the process. These findings provide a rational framework for designing continuous triphasic hydrogenation systems and contribute to the development of resource-efficient chemical technologies based on CO_2 utilization.

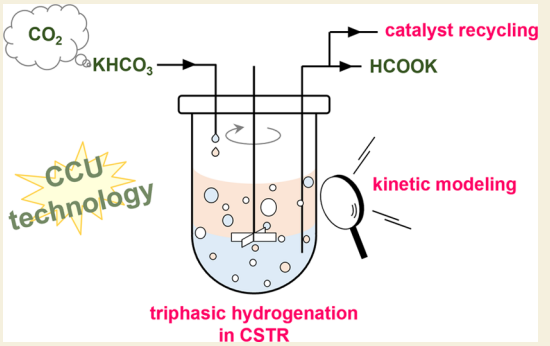

KEYWORDS: *CO_2 conversion, hydrogenation, catalyst recycling, Ru complex, continuous stirred-tank reactor, kinetic model*

INTRODUCTION

The establishment of a sustainable society through resource recycling has become one of the most critical global challenges in recent decades.[1] Among various approaches, the utilization of carbon dioxide (CO_2) as a C_1 building block has attracted significant attention, enabling the synthesis of valuable chemicals such as carbon monoxide,[2] formaldehyde,[3] methylformate,[4] methanol,[5] and methane.[6] In particular, the production of formic acid (HCOOH)[7] and formate ($HCOO^-$)[8] via hydrogenation of CO_2 or bicarbonate represents one of the most sustainable carbon capture and utilization (CCU) strategies since no hydrogen is lost as water during the reaction, and the products serve as industrially valuable chemical feedstocks, hydrogen carriers, and energy sources for fuel cells.[9] Recent studies have demonstrated the effectiveness of Ru-based homogeneous catalysts for CO_2 capture and hydrogenation (Figure 1). In 2014, Yadav et al. reported the hydrogenation of captured CO_2 using 1,8-diazabicyclo[5.4.0]undec-7-ene (DBU) in MeOH with $[RuCl_2(PPh_3)_3]$ as a catalyst to form methylformate, which was subsequently converted to formate via further hydrogenation with the same catalyst.[4a] The Pidko group also used DBU as a base to capture CO_2 and Ru complex **1** bearing a PNP-tridentate ligand as a catalyst for the hydrogenation.[10] Later, they established a gas−liquid−liquid triphasic system using the same Ru catalyst, enabling efficient hydrogenation of potassium bicarbonate ($KHCO_3$) derived from KOH and CO_2 (Figure 2).[11] In such triphasic systems, the resulting formate salts typically remain in the aqueous phase, while the organometallic catalyst stays in the organic phase, allowing for easy separation of the catalyst and products by simple decantation. Similarly, successful utilization of triphasic catalyst systems for CO_2 hydrogenation has been developed by the Prakash group,[8b,c] Scott et al.,[12] and Guan et al.[13] using other PNP-ligand Ru catalysts as shown in Figure 1.

Received: March 16, 2026
Revised: April 22, 2026
Accepted: April 23, 2026
Published: May 27, 2026

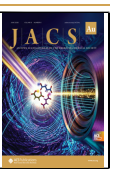

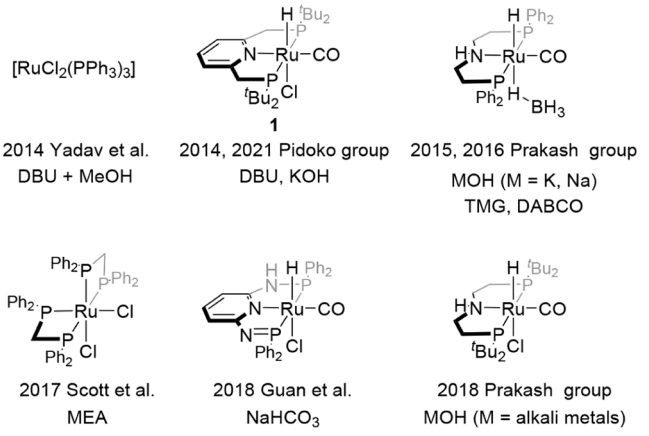

Figure 1. Representative Ru catalysts and CO_2 absorbents used in formate production via hydrogenation. DBU = 1,8-diazabicyclo[5.4.0]undec-7-ene, TMG = tetramethylguanidine, DABCO = diazabicyclo[2.2.2]octane, and MEA = monoethanolamine.

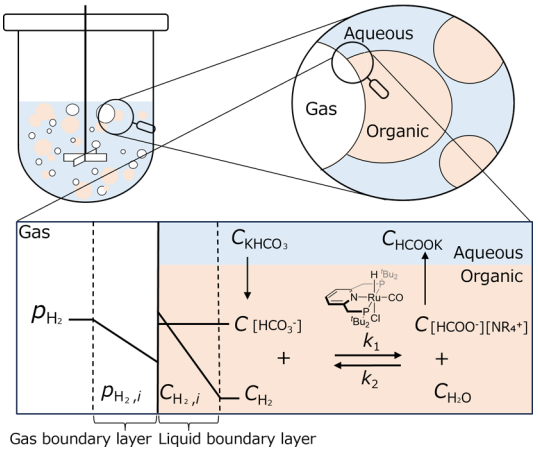

Figure 2. Triphasic reaction system consisting of an aqueous phase containing $KHCO_3$ and an organic phase containing Ru complex **1**, a quaternary ammonium salt (NR_4^+) as a phase-transfer catalyst (PTC), and the antioxidant tris(2,4-di-*tert*-butylphenyl)phosphite. A schematic of kinetic regimes and assumed concentration profiles at the gas–liquid interface and in the bulk phase, illustrating H_2 and $KHCO_3$.

Continuous synthesis plays a vital role in industrial chemical production, offering significant advantages in process efficiency, scalability, and cost reduction compared with conventional batch operations. Based on the hydrogenation of bicarbonate using Ru complex **1** in a batch reactor,[10,11] we previously examined the reaction under continuous-flow conditions using a tubular reactor to evaluate its performance and the recyclability of the catalyst.[14] The maximum formate yield (67%) was obtained with a 0.5 mol L^{-1} $KHCO_3$ aqueous phase; however, increasing the bicarbonate concentration to 1.25 mol L^{-1} and 1.5 mol L^{-1} resulted in lower formate yields of 33% and 31%, respectively. This decrease is likely due to mass transfer limitations among the three phases. To address similar challenges in triphasic hydrogenation systems, other groups have developed well-mixed continuous reactors, notably stirred-tank and jet-loop designs.[15−17] Continuous stirred-tank reactors (CSTRs) mitigate mass transfer limitations through uniform mixing and high interfacial area while offering a design similar to that of successful batch reactors, which simplifies scale-up and reduces development risk. Moreover, for reactor design, kinetic analysis is essential since it not only elucidates the underlying reaction mechanisms and rate-determining steps but also enables quantitative prediction of reaction rates under various operating conditions, which is essential for scale-up.[18] By establishing reliable rate expressions, it becomes possible to simulate and optimize reactor performance based on parameters such as temperature, pressure, and concentration. For instance, in such a triphasic system for the hydroformylation of 1-octene, it is known that the overall reaction rate is controlled by mechanical agitation, gas sparging, and residence time, which influence the environment at the liquid–liquid interface, gas–liquid interface, and within the bulk liquid phase.[19]

In continuous synthesis using flow reactors, maintaining catalyst activity over extended periods is essential for achieving a high production efficiency. However, flow systems are particularly susceptible to oxygen ingress through connection points, which can lead to catalyst deactivation. Accordingly, extensive research efforts have been devoted in both academia and industry to understanding and preventing catalyst deactivation, as it remains a critical challenge in long-term catalytic processes.[20−22] In our previous study, we reported that the antioxidant, tris(2,4-di-*tert*-butylphenyl)phosphite, effectively suppressed catalyst deactivation during $KHCO_3$ hydrogenation by preventing oxidation of the ligand caused by trace oxygen contamination.[11b] This strategy enabled the highest total turnover number (TON) reported to date for bicarbonate hydrogenation, reaching 9.43 million, and underscored the importance of oxidative stability in continuous reaction systems.

Building on this background and motivation, we herein established a kinetic model for the triphasic hydrogenation of $KHCO_3$ under high-pressure conditions, enabling the prediction of residence time vs yield relationships in a continuous stirred-tank reactor (CSTR). For gas–liquid reactions, diffusion of gaseous and liquid components and their subsequent reaction typically occur simultaneously within the liquid boundary layer near the gas–liquid interface. The relative magnitudes of diffusion and reaction rates determine the concentration profiles of reactants, thereby influencing the overall rate expression. In this study, the H_2 pressure was set at 50 bar to minimize the influence of interfacial mass transfer limitations (i.e., achieving sufficient supply of H_2 in the liquid phase, especially toward the gas–liquid interface), and the kinetics were formulated under the assumption that the overall reaction rate is governed by the catalytic reaction in the bulk liquid phase. Under these conditions, as illustrated in Figure 2, the concentration of dissolved H_2 decreases linearly across the boundary layer, while the $KHCO_3$ concentration remains constant. Here, C_{H_2} and C_{KHCO_3} are the concentrations of $KHCO_3$ and H_2, respectively, in the aqueous phase [mol m^{-3}], and p_{H_2} is the partial pressure of H_2 [Pa]. This situation corresponds to the "slow-reaction regime" in which residence time becomes the key design parameter, because the overall reaction rate is largely defined by the reaction rate in the bulk liquid and thus the reaction time can be effectively approximated by the residence time, i.e., how long reactants remain in the continuous reactor.[23,24] The developed kinetic model exhibited excellent agreement with the experimental

https://doi.org/10.1021/jacsau.6c00388
JACS Au 2026, 6, 3386−3393

data, demonstrating that high formate yields can be achieved in a CSTR through residence-time optimization. Furthermore, phase separation and catalyst recycling were successfully demonstrated within the same flow system, establishing a rational and scalable foundation for the industrial implementation of triphasic hydrogenation.

RESULTS AND DISCUSSIONS

Kinetic Modeling Using Batch Reaction Data

As the initial step of this study, we developed and validated a kinetic model for the hydrogenation of $KHCO_3$ to potassium formate (HCOOK) (eq 1) based on general reaction kinetics in gas−liquid biphasic systems

$$KHCO_3 + H_2 \leftrightarrows HCOOK + H_2O \quad (1)$$

As illustrated in Figure 2, under the present reaction conditions, the overall reaction rate was assumed to be governed by the catalytic reaction in the bulk liquid phase, while mass transfer across the gas and liquid films was balanced with the bulk reaction rate. Based on the molar balance, eq 2 is obtained with the assumptions that the hydrogen absorption rate into the liquid phase is equal to the formate production rate as well as the potassium bicarbonate consumption rate

$$\begin{aligned} -r_{H_2} &= k_G \cdot a_b \cdot (p_{H_2} - p_{H_2,i}) \\ &= k_L \cdot a_b \cdot (C_{H_2,i} - C_{H_2}) \\ &= k_1 \cdot C_{H_2} \cdot C_{KHCO_3} - k_2 \cdot (C_{KHCO_3[0]} - C_{KHCO_3}) \end{aligned} \quad (2)$$

Here, the H_2 consumption rate per unit volume was expressed as $-r_{H_2}$ [mol m^{-3} s^{-1}]. The parameters k_G [mol m^{-2} s^{-1} Pa^{-1}] and k_L [m s^{-1}] represent the gas- and liquid-side mass transfer coefficients, respectively. The hydrogen partial pressure is denoted as p_{H_2} [Pa], and the gas−liquid interfacial area is represented by a_b [m^2 m^{-3}]. Moreover, the net reaction rate in the bulk liquid phase is determined by the forward and reverse reaction rates, where k_1 [mol m^{-3} s^{-1}] and k_2 [s^{-1}] are the respective rate constants. In the reverse reaction term, the concentration of water was assumed to remain effectively constant because water was present in large excess in the aqueous phase; therefore, the reverse reaction was treated as pseudo-first-order with respect to formate concentration. This approximation may not hold if the water content changes significantly. The subscript "i" refers to the concentration or partial pressure at the gas−liquid interface (film region), while "$C_{KHCO_3[0]}$" denotes the initial concentration of $KHCO_3$ in the aqueous phase.

The equilibrium relationship between the partial pressure of hydrogen in the gas phase and its concentration in the liquid phase is described by Henry's law, as shown in eq 3:

$$p_{H_2,i} = H_{H_2} \cdot C_{H_2,i} \quad (3)$$

Here, $p_{H_2,i}$ represents the partial pressure of hydrogen in the gas phase [Pa], $C_{H_2,i}$ denotes the concentration of dissolved hydrogen in the liquid phase [mol m^{-3}], and H_{H_2} is the Henry's constant for hydrogen [Pa m^3 mol^{-1}]. This equation quantitatively describes the solubility equilibrium of H_2, indicating that its partial pressure is directly proportional to its concentration in the liquid phase.

The reverse reaction rate is defined as being proportional to the forward reaction rate constant, and the proportionality factor α is given by the following ratio (eq 4):

$$\alpha = \frac{k_2}{k_1} \quad (4)$$

Substituting eq 3 into eq 2 yields a function of $C_{H_2,i}$, eliminating $p_{H_2,i}$. Further mathematical transformation leads to eq 5, in which the consumption rates of $KHCO_3$ and H_2 are equal (see SI for detailed derivation):

$$\begin{aligned} -r_{H_2} &= -r_{KHCO_3} \\ &= \frac{p_{H_2} \cdot C_{KHCO_3} + \boldsymbol{C} \cdot (C_{KHCO_3} - C_{KHCO_3[0]})}{\boldsymbol{A} \cdot C_{KHCO_3} + \boldsymbol{B}} \end{aligned} \quad (5)$$

where the parameters are defined as

$$\boldsymbol{A} = \frac{1}{a_b \cdot k_G} + \frac{H_{H_2}}{a_b \cdot k_L} [\text{Pa s mol}^{-1}]$$

$$\boldsymbol{B} = \frac{H_{H_2}}{k_1} [\text{Pa s}]$$

$$\boldsymbol{C} = H_{H_2} \cdot \alpha [\text{Pa}]$$

Here, $-r_{KHCO_3}$ [mol m^{-3} s^{-1}] represents the consumption rate of $KHCO_3$ per unit liquid volume.

To evaluate the proposed kinetic model, batch hydrogenation of $KHCO_3$ was conducted under various conditions, including substrate concentration ($C_{KHCO_3[0]}$ = 2.0−3.6 mol L^{-1}), catalyst concentration ($C_{Ru\ catalyst}$ = 60−240 μmol L^{-1}), and H_2 pressure (30−50 bar), as summarized in Table 1.

Table 1. Summary of the Experimental Conditions Used for Kinetic Validation[a,b,c,d,e]

entry	$C_{KHCO_3[0]}$ [mol L^{-1}]	$C_{Ru\ catalyst}$ [μmol L^{-1}]	H_2 pressure [bar]	formate yield after 2.5 h [%]
1	3.6	120	40	75
2	3.6	60	40	70
3	3.6	240	40	72
4	3.6	120	30	65
5	3.6	120	50	73
6	2.0	60	50	66

[a]Batch hydrogenation of $KHCO_3$ was performed at varying substrate concentrations, catalyst loadings, and H_2 pressures (entries 1−6). [b]Reaction conditions: the organic phase contained 60−120 μmol L^{-1} Ru complex **1**, 54 mmol L^{-1} trioctylmethylammonium chloride, and 6 mmol L^{-1} tris(2,4-di-*tert*-butylphenyl)phosphite; the aqueous phase contained 2.0−3.6 mol L^{-1} $KHCO_3$. [c]H_2 pressure was 30−50 bar. [d]50 mL toluene and 50 mL aqueous. [e]Reaction time = 90−120 min.

Formate was obtained in comparable yields (65−75%) after 2.5 h (Table 1), while the reaction rates varied depending on the conditions (see Figure S1 for raw reaction rate data). The kinetic parameters ***A***, ***B***, and ***C*** were estimated by fitting the experimental data to eq 5 using nonlinear least-squares optimization, which minimized the residuals between the measured and simulated $KHCO_3$ concentrations over time. To ensure an accurate representation of the primary reaction phase, fitting was performed using conversion data up to 10% below the final yield. No side products were detected through

https://doi.org/10.1021/jacsau.6c00388
JACS Au 2026, 6, 3386−3393

the experiments, confirming the high selectivity of the hydrogenation. As shown in the parity plot (Figure 3), the

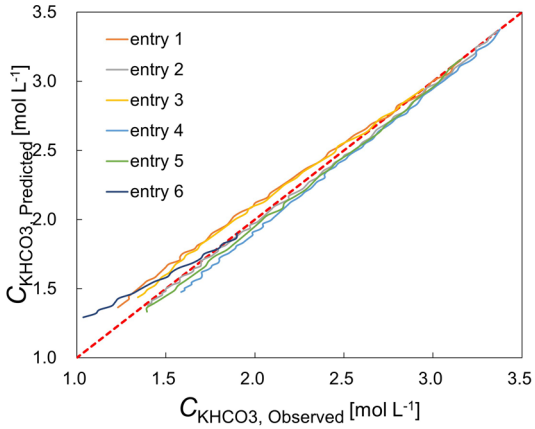

Figure 3. Parity plot of measured versus simulated concentrations of $KHCO_3$ under various hydrogenation conditions. The close alignment with the diagonal line confirms the validity of the proposed kinetic model.

model demonstrated excellent predictive performance under all tested conditions, with data points closely aligned along the diagonal ($y = x$), indicating strong agreement between experimental results and model predictions. For example, at a Ru complex **1** of 60 μmol L^{-1}, the fitted parameters were $\boldsymbol{A}$ = 3.47 × 10^6 [Pa s mol^{-1}], $\boldsymbol{B}$ = 9.66 × 10^9 [Pa s], and $\boldsymbol{C}$ = 6.36 × 10^5 [Pa].

The single-pass conversion of $KHCO_3$ is defined as $x = (C_{in} - C_{out})/C_{in}$, corresponding to the formate yield under the assumption of 100% selectivity, which was confirmed by our experiment within the detection limit. Subsequently, the relationship between the residence time and formate yield was predicted using the developed kinetic model, as illustrated in Figure 4. These insights provided the basis for applying the model to a CSTR reactor, enabling further evaluation under flow conditions.

Flow Reaction

Next, we prepared a CSTR bearing a custom-built 200 mL vessel with a height of 90 mm and a diameter of 56 mm,

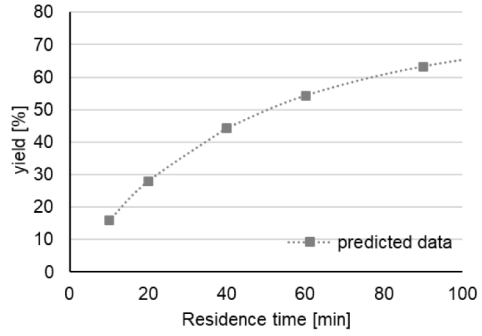

Figure 4. Predicted formate yield as a function of residence time in CSTR on the overall reaction rate equation with constants $\boldsymbol{A}$ = 3.47 × 10^6 [Pa s mol^{-1}], $\boldsymbol{B}$ = 9.66 × 10^9 [Pa s], and $\boldsymbol{C}$ = 6.36 × 10^5 [Pa]. Conditions: The organic phase contained 60 μmol L^{-1} Ru complex **1**, 2 mol L^{-1} $KHCO_3$ and 50 bar of H_2 pressure.

Application of Kinetic Parameters to Predict CSTR Performance

Based on the reaction kinetics established through batch experiments, a kinetic model for a CSTR was developed. Under steady-state conditions and assuming perfect mixing, the material balance for $KHCO_3$ in the CSTR is expressed as follows:

$$F_{A0} - F_A = \nu(C_{in} - C_{out}) = -r_A V \tag{6}$$

Where F_{A0} and F_A are the inlet and outlet molar flow rates [mol s^{-1}], C_{in} and C_{out} are the inlet and outlet concentrations [mol m^{-3}], ν is the volumetric flow rate [m^3 s^{-1}], V is the reactor liquid volume [m^3], and $\tau = V/\nu$ is the residence time [s]. Substituting eq 5 into eq 6 and rearranging yields eq 7:

$$C_{in} - C_{out} = \tau \frac{p_{H_2} C_{out} + \boldsymbol{C}(C_{out} - C_{in})}{\boldsymbol{A}C_{out} + \boldsymbol{B}} \tag{7}$$

Further algebra manipulation of eq 7 leads to eq 8:

$$C_{out} = \frac{\boldsymbol{A}C_{in} - \{\boldsymbol{B} + \tau(p_{H_2} + \boldsymbol{C})\} + \sqrt{\{\boldsymbol{B} + \tau(p_{H_2} + \boldsymbol{C}) - \boldsymbol{A}C_{in}\}^2 + 4\boldsymbol{A}C_{in}(\boldsymbol{B} + \tau\boldsymbol{C})}}{2\boldsymbol{A}} \tag{8}$$

equipped with a 20 mm four-blade stirring wing positioned at the interface between the 20 mL of organic and 20 mL of aqueous phases (Figures 5and S2). Prior to each experiment, the reactor was flushed with N_2, the pressure of which was adjusted with a rotameter. The organic phase was prepared in a glovebox under a nitrogen atmosphere using degassed toluene containing Ru complex **1**, trioctylmethylammonium chloride, and tris(2,4-di-*tert*-butylphenyl)phosphite. The aqueous phase was prepared using standard Schlenk techniques with degassed distilled water containing 2 mol L^{-1} of $KHCO_3$ under argon. Those prepared solutions were filled into canisters, which were connected to the stirred tank, and a total of 40 mL of the organic and aqueous phases was introduced. The mixture in the reactor was pressurized with H_2 to 50 bar and then heated to 90 °C and stirred for a designated period. Continuous operation was initiated by simultaneously feeding and withdrawing both phases at controlled flow rates. The resulted mixture was collected to a phase separator to sample the aqueous phase containing formate while recycling the organic phase, which contains the catalyst.

The mixing behavior within the reactor was initially assessed by direct visual inspection, made possible by the incorporation of a sapphire view cell into the reactor design (Figure 5B). This approach is notably rare in high-pressure CSTRs, where internal observation is typically restricted due to system constraints. The ability to visually monitor the mixing process under actual operating conditions allowed for direct evaluation of phase behavior and facilitated the optimization of both the stirring blade position and rotation speed. This was particularly important in the three-phase reaction system, where efficient interfacial mixing is essential for enhancing mass transfer

https://doi.org/10.1021/jacsau.6c00388
JACS Au 2026, 6, 3386−3393

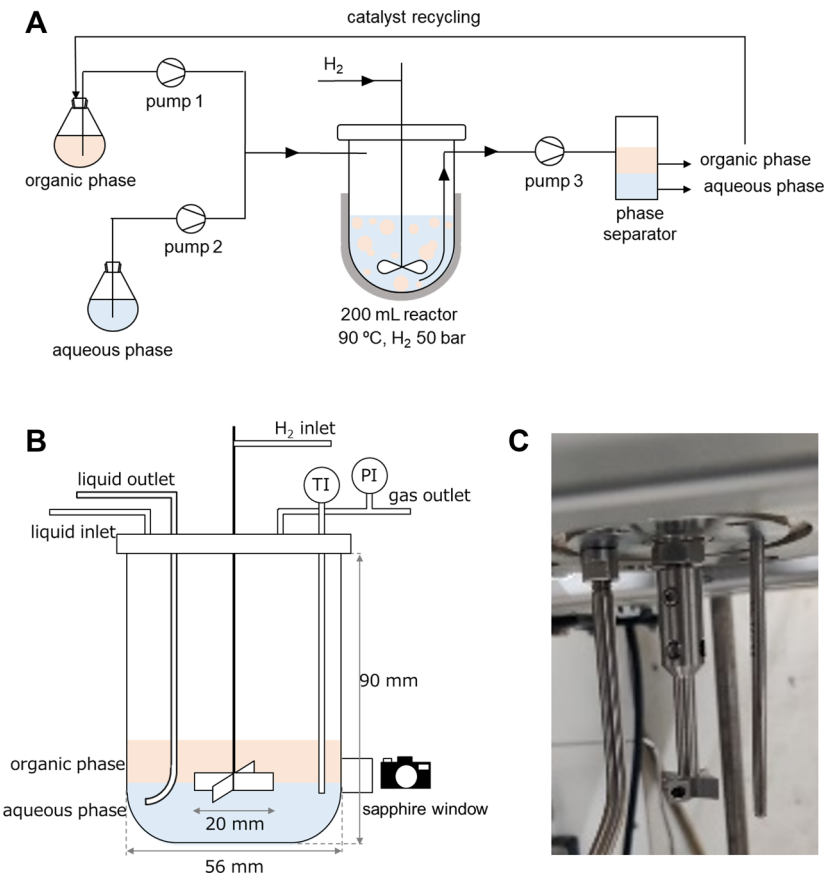

Figure 5. (**A**) Simplified diagram of the CSTR. (**B**) Schematic diagram of the stirred tank reactor for the hydrogenation of $KHCO_3$. (**C**) Stirring wing.

between phases and improving the overall reaction efficiency. At a stirring rate of 300 rpm, the organic and aqueous phases remained clearly separated, while uniform mixing of the two phases was observed at stirring rates of 600 rpm or higher (Figure 6). Moreover, stirring at 800 rpm was necessary to achieve homogeneous mixing and sample the mixture with the desired ratio of the organic to aqueous phase.

Next, to evaluate the effect of the phase volume ratio in the reactor, the ratio between the organic and aqueous phases was varied upon different catalyst loadings while maintaining a constant total volume of 40 mL and a constant residence time (Table 2). At a 1:1 organic-to-aqueous phase ratio and a residence time of 60 min, the collected aqueous phase through pump 3 (Figure 5A) showed a 26% formate yield (entry 1). On the other hand, when the volumes of each phase were adjusted to 8 mL of organic phase and 32 mL of aqueous phase, the formic acid yield decreased to 18% (entry 2), even at a catalyst loading higher than that in entry 1 (entry 2). The vertical position of the stirring blades close to the phase interface (under the static case—organic phase above and aqueous phase below) was found at the 1:1 ratio, presumably enhancing interfacial mass transfer and resulting in improved overall catalytic reaction efficiency (see Figure S3). Thus, the 1:1 phase ratio was selected for subsequent experiments. The effects of the phase volume ratio on reaction performance were systematically evaluated in a batch reactor, as summarized in Figures S4 and S5 and Tables S2 and S3.

Table 2. Effect of Phase Volume Ratio in the Reactor with Different Ru Complex Loading[a,b,c,d]

entry	organic phase [mL]	aqueous phase [mL]	Ru complex **1** [μmol L^{-1}[e]]	formate yield [%]
1	20	20	30	26
2	8	32	50	18

[a]Organic phase: [Ru complex **1**] = 60 or 250 μmol L^{-1} (Overall Ru concentration in the reactor: 30 μmol L^{-1} (entry 1), 50 μmol L^{-1} (entry 2)), [trioctylmethylammonium chloride] = 54 mmol L^{-1}, [tris(2,4-di-*tert*-butylphenyl)phosphite] = 6 mmol L^{-1}. [b]Aqueous phase: [$KHCO_3$] = 2 mol L^{-1}. [c]H_2 pressure was 50 bar. [d]Residence time: 60 min. [e]Calculated based on the total liquid volume (organic + aqueous phase) in the reactor.

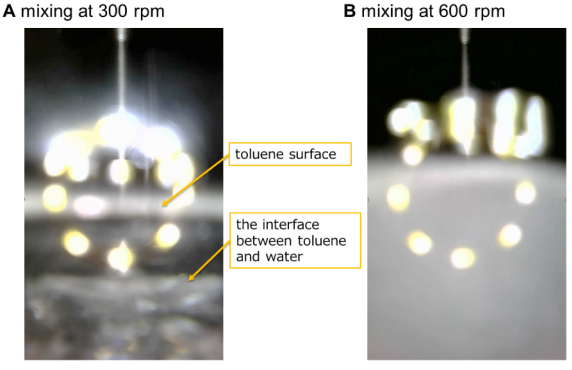

Figure 6. Liquid-phase behavior of toluene and water at 300 rpm (**A**) and 600 rpm (**B**) in the CSTR. Those figures were taken from a view port of the CSTR.

https://doi.org/10.1021/jacsau.6c00388
JACS Au 2026, 6, 3386−3393

To evaluate the reusability of the catalyst, recycling experiments were performed by introducing 20 mL of each of the organic and aqueous phases into the reactor (Figure 7).

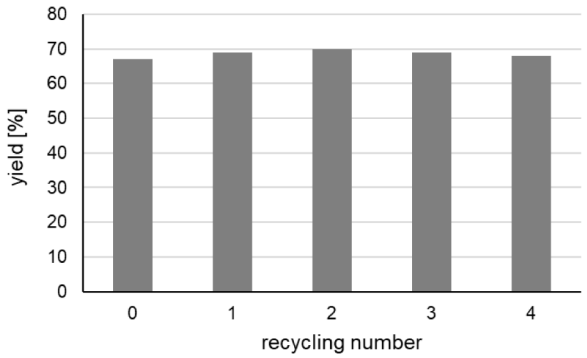

Figure 7. Catalyst recycling experiment on the continuous flow reaction. Reaction conditions: organic phase contained 60 μmol L^{-1} Ru complex **1**, 54 mmol L^{-1} trioctylmethylammonium chloride, and 6 mmol L^{-1} tris(2,4-di-*tert*-butylphenyl)phosphite; aqueous phase contained 2 mol L^{-1} $KHCO_3$. H_2 pressure was 50 bar. Phase volumes in the reactor: 20 mL of organic and 20 mL of aqueous. Residence time: 90 min.

Initially, the hydrogenation of $KHCO_3$ was first carried out as a batch reaction for 90 min to reach equilibrium, after which the system was switched to continuous operation with a residence time of 90 min. Following each reaction, the organic phase was collected, diluted to its original volume, and stored for 20 h. The recovered organic phase was then used in the subsequent continuous-flow experiment combined with a fresh aqueous phase.

The catalyst storage conditions were optimized through both batch and flow hydrogenation reaction (see Tables S5 and S6). A clear difference in catalyst stability was observed depending on the storage atmosphere. The Ru catalyst stored under a hydrogen atmosphere exhibited higher stability than that stored under nitrogen. ^{1}H NMR measurements revealed that pressurization of the organic phase with H_2 led to the formation of Ru dihydrido and formate complexes with suppressing the decomposition of complex **1** (Figure S6). Moreover, the stability of the isolated Ru formate complex was examined (Figure S8). A solution of the Ru formate complex in C_6D_6 was stirred with 1 mL of a 5 mol L^{-1} D_2O solution of HCOOK for 30 min. The obtained organic phase was subsequently divided into two portions and stored for 4 days under either a hydrogen or nitrogen atmosphere at 6 bar. For the sample stored under nitrogen, decomposition of Ru complexes was observed (Figure S8a), whereas the sample stored under hydrogen retained complex **1** and the formate complex (Figure S8b). Furthermore, the addition of 6 mmol L^{-1} tris(2,4-di-*tert*-butylphenyl)phosphite to the organic phase significantly increased the formate yield in the subsequent reaction, likely due to suppression of oxidation of the PNP ligand.[11b] Under the optimized condition with a residence time of 90 min, the formate yield reached 67−70% over four recycling tests (total TON = 114 × 10^3), showing good agreement with the model predictions. Formate yields were calculated using the aqueous phase collected from the reactor after each reaction since it is the yield during the steady-state reaction. As shown in Table S4, the time-dependent formate yields indicate that the formate yield was 39% in the initial aqueous phase collected at 90 min, whereas it increased to 60% in the later aqueous phase collected at 150 min. These results indicate that a certain period is required for the system to reach steady state and that the aqueous phase collected from the reactor represents the composition at a given steady-state condition. Additional catalyst recycling data are provided in the Supporting Information (Tables S7−S10).

To verify catalyst recovery, ICP-MS analysis was conducted to quantify the Ru content in each phase. When the initial Ru concentration in the organic phase was 60 μmol L^{-1}, the Ru concentration in the organic phase remained unchanged after hydrogenation. However, approximately 3% of the Ru originally present in the organic phase was detected in the collected aqueous phase, which can be attributed to the partial transfer of the organic phase itself into the aqueous phase rather than intrinsic leaching of the Ru catalyst. In Figure 7, 47 mL of the organic phase was recovered from an initial volume of 60 mL after the first reaction, while an additional 5−8 mL of the organic phase could not be recovered in subsequent recycling runs (Table S10). The loss of the organic phase is attributed to two main factors: partial dispersion of the organic phase into the aqueous phase during the reaction and retention of a portion of the organic phase in the reactor and tubing.

In conclusion, we successfully established a CSTR system for the hydrogenation of $KHCO_3$ under high-pressure conditions. By visually confirming and optimizing the stirring conditions using a view cell, we ensured efficient mixing, which is essential for maintaining the reaction performance in the triphasic flow system. Furthermore, by analyzing the batch reaction data within a unified kinetic framework that assumes a slow-reaction regime and consideration of the reverse reaction, a consistent set of kinetic parameters was obtained. These parameters were applied to the CSTR model, enabling reliable prediction of the residence time−yield relationship. A kinetic model developed from batch experiments accurately predicted the residence time−yield relationship in the CSTR, with formate yields closely matching the model's predictions. Regarding scalability, the current model is based on a well-mixed stirred tank and incorporates interfacial and transport parameters and is therefore expected to remain applicable at larger scales provided hydrodynamic and mass-transfer performance are preserved. In practice, this requires maintaining power input per unit volume and matching the overall gas−liquid mass-transfer coefficient under geometric similarity. For pilot or industrial translation, we recommend verifying the gas−liquid mass-transfer coefficient and assessing dispersion characteristics to ensure stable operation. These measures provide a practical framework for scaling continuous triphasic hydrogenation processes based on CO_2 utilization.

■ ASSOCIATED CONTENT

Supporting Information

The Supporting Information is available free of charge at https://pubs.acs.org/doi/10.1021/jacsau.6c00388.

Experimental procedures, kinetic model derivation, supplemental results for batch and flow hydrogenation, including liquid phase-ratio effects and steady-state confirmation, catalyst storage and recycling data, and NMR spectra (PDF)

https://doi.org/10.1021/jacsau.6c00388
JACS Au 2026, 6, 3386−3393

AUTHOR INFORMATION

Corresponding Authors

Makoto Hirano − *Separation Technology Research Center, Corporate Research and Development Division, Nitto Denko Corporation, Osaka 567−8680, Japan;* orcid.org/0009-0004-3008-1670; Email: makoto.hirano@nitto.com

Atsushi Urakawa − *Catalysis Engineering, Department of Chemical Engineering, Delft University of Technology, Delft 2629 HZ, The Netherlands;* orcid.org/0000-0001-7778-4008; Email: A.Urakawa@tudelft.nl

Authors

Mariko Inoue − *Separation Technology Research Center, Corporate Research and Development Division, Nitto Denko Corporation, Osaka 567−8680, Japan;* orcid.org/0000-0002-0752-5593

Gul Afreen − *Catalysis Engineering, Department of Chemical Engineering, Delft University of Technology, Delft 2629 HZ, The Netherlands*

Kazuhito Wada − *Separation Technology Research Center, Corporate Research and Development Division, Nitto Denko Corporation, Osaka 567−8680, Japan*

Matteo Tafuro − *Catalysis Engineering, Department of Chemical Engineering, Delft University of Technology, Delft 2629 HZ, The Netherlands*

Kodai Nogami − *Separation Technology Research Center, Corporate Research and Development Division, Nitto Denko Corporation, Osaka 567−8680, Japan*

Evgeny A. Uslamin − *Catalysis Engineering, Department of Chemical Engineering, Delft University of Technology, Delft 2629 HZ, The Netherlands;* orcid.org/0000-0001-5454-9582

Atul Bansode − *Catalysis Engineering, Department of Chemical Engineering, Delft University of Technology, Delft 2629 HZ, The Netherlands;* orcid.org/0000-0002-1972-6704

Hideaki Tsuneki − *Department of Applied Chemistry, Waseda University, Tokyo 169-8555, Japan*

Complete contact information is available at: https://pubs.acs.org/10.1021/jacsau.6c00388

Author Contributions

#M.I. and G.A. contributed equally.

Notes

The authors declare no competing financial interest.

ACKNOWLEDGMENTS

We appreciate Harrie Jansma for his help in building the CSTR and Masaya Seriu for fruitful discussions.

REFERENCES

(1) (a) Selected reviews for CO_2 utilization: Jessop, P. G.; Ikariya, T.; Noyori, R. Homogeneous Hydrogenation of Carbon Dioxide. *Chem. Rev.* **1995**, *95*, 259−272. (b) Leitner, W. Carbon Dioxide as a Raw Material: The Synthesis of Formic Acid and Its Derivatives from CO2. *Angew. Chem. Int. Ed. Engl* **1995**, *34*, 2207−2221. (c) Liu, Q.; Wu, L.; Jackstell, R.; Beller, M. Using carbon dioxide as a building block in organic synthesis. *Nat. Commun* **2015**, *6*, 5933. (d) Wang, W.-H.; Himeda, Y.; Muckerman, J. T.; Manbeck, G. F.; Fujita, E. CO2 Hydrogenation to Formate and Methanol as an Alternative to Photo- and Electrochemical CO2 Reduction. *Chem. Rev* **2015**, *115*, 12936−12973. (e) Li, Y.; Cui, X.; Dong, K.; Junge, K.; Beller, M. Utilization of CO_2 as a C1 Building Block for Catalytic Methylation Reactions. *ACS Catal* **2017**, *7*, 1077−1086. (f) Kar, S.; Kothandaraman, J.; Goeppert, A.; Prakash, G. K. S. Advances in catalytic homogeneous hydrogenation of carbon dioxide to methanol. *J. CO2 Util* **2018**, *23*, 212−218. (g) Kuramochi, Y.; Ishitani, O.; Ishida, H. Reaction mechanisms of catalytic photochemical CO2 reduction using Re(I) and Ru(II) complexes. *Coord. Chem. Rev* **2018**, *373*, 333−356. (h) Kar, S.; Goeppert, A.; Prakash, G. K. S. Integrated CO_2 Capture and Conversion to Formate and Methanol: Connecting Two Threads. *Acc. Chem. Res* **2019**, *52*, 2892−2903. (i) Mohsin, I.; Al-Attas, T. A.; Sumon, K. Z.; Bergerson, J.; McCoy, S.; Kibria, M. G. Economic and Environmental Assessment of Integrated Carbon Capture and Utilization. *Cell Rep. Phys. Sci* **2020**, *1*, 100104. (j) Sen, R.; Goeppert, A.; Surya Prakash, G. K. Homogeneous Hydrogenation of CO_2 and CO to Methanol: The Renaissance of Low-Temperature Catalysis in the Context of the Methanol Economy. *Angew. Chem., Int. Ed* **2022**, *61*, No. e202207278. (k) Wei, D.; Sang, R.; Moazezbarabadi, A.; Junge, H.; Beller, M. Homogeneous Carbon Capture and Catalytic Hydrogenation: Toward a Chemical Hydrogen Battery System. *JACS Au* **2022**, *2*, 1020−1103. (l) Siegel, R. E.; Pattanayak, S.; Berben, L. A. Reactive Capture of CO2: Opportunities and Challenges. *ACS Catal* **2023**, *13*, 766−784. (m) Choudhury, J.; Bhardwaj, R.; Mandal, S. K. Hydride Transfer-Based CO2 Reduction Catalysis: Navigating Metal Hydride to Organic Hydride in the Catalytic Loop. *Acc. Chem. Res* **2024**, *57*, 2859−2871. (n) Langie, K.; Bak, G.; Lee, U.; Lee, D. K.; Lee, C. W.; Hwang, Y. J.; Won, D. H. Advances in the direct electro-conversion of captured CO2 into valuable products. *J. Mater. Chem. A* **2024**, *12*, 10597−10613. (o) Peng, Y.; Alberico, E.; Junge, H.; Beller, M. Homogeneous catalytic hydrogenation of CO_2 − amino acid-based capture and utilization. *Chem. Soc. Rev* **2025**, *54*, 5551−5585.

(2) (a) Selected recent reviews on CO_2 conversion to CO: Bahmanpour, A. M.; Signorile, M.; Kröcher, O. Recent progress in syngas production via catalytic CO2 hydrogenation reaction. *Appl. Catal., B* **2021**, *295*, 120319. (b) Triviño, M. L. T.; Arriola, N. C.; Kang, Y. S.; Seo, J. G. Transforming CO_2 to valuable feedstocks: Emerging catalytic and technological advances for the reverse water gas shift reaction. *Chem. Eng. J* **2024**, *487*, 150369.

(3) (a) Selected studies on CO_2 conversion to formaldehyde: Rauch, M.; Strater, Z.; Parkin, G. Selective Conversion of Carbon Dioxide to Formaldehyde via a Bis(silyl)acetal: Incorporation of Isotopically Labeled C1Moieties Derived from Carbon Dioxide into Organic Molecules. *J. Am. Chem. Soc* **2019**, *141*, 17754−17762. (b) Zhao, S.; Liang, H.-Q.; Hu, X.-M.; Li, S.; Daasbjerg, K. Challenges and Prospects in the Catalytic Conversion of Carbon Dioxide to Formaldehyde. *Angew. Chem., Int. Ed* **2022**, *61*, No. e202204008.

(4) (a) Yadav, M.; Linehan, J. C.; Karkamkar, A. J.; van der Eide, E.; Heldebrant, D. J. Selected studies on CO_2 conversion to methylformate: Yadav. *Inorg. Chem* **2014**, *53*, 9849−9854. (b) Cor-ral-Perez, J.-J.; Bansode, A.; Praveen, C. S.; Kokalj, A.; Reymond, H.; Comas-Vives, A.; VandeVondele, J.; Copéret, C.; von Rohr, R. R.; Urakawa, A. *J. Am. Chem. Soc.* **2018**, *140*, 13884−13891. (c) Jens, C. M.; Müller, L.; Leonhard, K.; Bardow, A. To Integrate or Not to Integrate—Techno-Economic and Life Cycle Assessment of CO2 Capture and Conversion to Methyl Formate Using Methanol. *ACS Sustainable Chem. Eng* **2019**, *7*, 12270−12280. (d) Park, H.; Park, K.; Jung, K.-D.; Yoon, S. CO_2 hydrogenation into formate and methyl formate using Ru molecular catalysts supported on *NNN* pincer porous organic polymers. *Inorg. Chem. Front* **2021**, *8*, 1727−1735.

(5) (a) Selected studies and reviews on CO_2 conversion to methanol: Kothandaraman, J.; Goeppert, A.; Czaun, M.; Olah, G. A.; Prakash, G. K. S. Conversion of CO_2 from Air into Methanol Using a Polyamine and a Homogeneous Ruthenium Catalyst. *J. Am. Chem. Soc.* **2016**, *138*, 778−781. (b) Olah, G. A.; Mathew, T.; Prakash, G. K. S. Chemical Formation of Methanol and Hydrocarbon ("Organic") Derivatives from CO2 and H2—Carbon Sources for Subsequent Biological Cell Evolution and Life's Origin. *J. Am. Chem. Soc* **2017**, *139*, 566−570. (c) Kar, S.; Sen, R.; Goeppert, A.; Prakash, G. K. S. Integrative CO2 Capture and Hydrogenation to Methanol with

Reusable Catalyst and Amine: Toward a Carbon Neutral Methanol Economy. *J. Am. Chem. Soc* **2018**, *140*, 1580−1583. (d) Kar, S.; Sen, R.; Kothandaraman, J.; Goeppert, A.; Chowdhury, R.; Munoz, S. B.; Haiges, R.; Prakash, G. K. S. Mechanistic Insights into Ruthenium-Pincer-Catalyzed Amine-Assisted Homogeneous Hydrogenation of CO_2 to Methanol. *J. Am. Chem. Soc* **2019**, *141*, 3160−3170. (e) Sen, R.; Goeppert, A.; Kar, S.; Prakash, G. K. S. Hydroxide Based Integrated CO2 Capture from Air and Conversion to Methanol. *J. Am. Chem. Soc* **2020**, *142*, 4544−4549.

(6) (a) Selected recent reviews on CO_2 conversion to methane: Lee, W. J.; Li, C.; Prajitno, H.; Yoo, J.; Patel, J.; Yang, Y.; Lim, S. Recent trend in thermal catalytic low temperature CO2 methanation: A critical review. *Catal. Today* **2021**, *368*, 2−19. (b) Pham, C. Q.; Bahari, M. B.; Kumar, P. S.; Ahmed, S. F.; Xiao, L.; Kumar, S.; Qazaq, A. S.; Siang, T. J.; Tran, H.-T.; Islam, A.; et al. RETRACTED ARTICLE: Carbon dioxide methanation on heterogeneous catalysts: a review. *Environ. Chem. Lett* **2022**, *20*, 3613−3630. (c) Ullah, S.; Gao, Y.; Dou, L.; Liu, Y.; Shao, T.; Yang, Y.; Murphy, A. B. Recent Trends in PlasmaAssisted CO_2 Methanation: A Critical Review of Recent Studies. *Plasma Chem. Plasma Process* **2023**, *43*, 1335−1383.

(7) (a) selected recent studies on CO_2 conversion to formic acid: Li, Y.-N.; He, L.-N.; Lang, X.-D.; Liu, X.-F.; Zhang, S. An integrated process of CO2 capture and in situ hydrogenation to formate using a tunable ethoxylfunctionalized amidine and Rh/bisphosphine system. *RSC Adv.* **2014**, *4*, 49995−50002. (b) Hsu, S.-F.; Rommel, S.; Eversfield, P.; Muller, K.; Klemm, E.; Thiel, W. R.; Plietker, B. A Rechargeable Hydrogen Battery Based on Ru Catalysis. *Angew. Chem., Int. Ed* **2014**, *53*, 7074−7078. (c) Kim, C.; Park, K.; Lee, H.; Im, J.; Ususky, D.; Tak, K.; Park, D.; Chung, W.; Han, D.; Yoon, J.; et al. Accelerating the net-zero economy with CO2-hydrogenated formic acid production: Process development and pilot plant demonstration. *Joule* **2024**, *8*, 693−713.

(8) (a) Selected studies on CO2 conversion to formate: Li, Y.-N.; He, L.-N.; Liu, A.-H.; Lang, X.-D.; Yang, Z.-Z.; Yua, B.; Luan, C.-R. *In situ* hydrogenation of captured CO2 to formate with polyethyleneimine and Rh/monophosphine system. *Green Chem* **2013**, *15*, 2825−2829. (b) Kothandaraman, J.; Goeppert, A.; Czaun, M.; Olah, G. A.; Surya Prakash, G. K. CO_2 capture by amines in aqueous media and its subsequent conversion to formate with reusable ruthenium and iron catalysts. *Green Chem* **2016**, *18*, 5831−5838. (c) Kar, S.; Goeppert, A.; Galvan, V.; Chowdhury, R.; Olah, J.; Prakash, G. K. S. A Carbon-Neutral CO2 Capture, Conversion, and Utilization Cycle with Low-Temperature Regeneration of Sodium Hydroxide. *J. Am. Chem. Soc* **2018**, *140*, 16873−16876. (d) Yoon, H.; Park, K.; Jung, K.-D.; Yoon, S. Simultaneous utilization of CO2 and potassium-rich biomass for the environmentally friendly production of potassium formate. *RSC Adv* **2025**, *15*, 348−356.

(9) Schuler, E.; Morana, M.; Ermolich, P. A.; Lüschen, K.; Greer, A. J.; Taylor, S. F. R.; Hardacre, C.; Shiju, N. R.; Gruter, G.-J. M. Formate as a key intermediate in CO_2 utilization. *Green Chem* **2022**, *24*, 8227−8258.

(10) Filonenko, G. A.; van Putten, R.; Schulpen, E. N.; Hensen, E. J. M.; Pidko, E. A. Highly Efficient Reversible Hydrogenation of Carbon Dioxide to Formates Using a Ruthenium PNP-Pincer Catalyst. *ChemCatChem* **2014**, *6*, 1526−1530.

(11) (a) Rebreyend, C.; Pidko, E. A.; Filonenko, G. A. Homogeneous hydrogenation of saturated bicarbonate slurry to formates using multiphase catalysis. *Green Chem* **2021**, *23*, 8848−8852. (b) Hirano, M.; Wada, K.; Matsuda, H.; Pidko, E. A. Antioxidant-driven activity and stability enhancement in multiphase bicarbonate hydrogenation catalysis with a Ru-PNP pincer complex. *J. CO2 Util* **2024**, *81*, 102718.

(12) Scott, M.; Molinos, B. B.; Westhues, C.; Franciò, G.; Leitner, W. Aqueous Biphasic Systems for the Synthesis of Formates by Catalytic CO2 Hydrogenation: Integrated Reaction and Catalyst Separation for CO2-Scrubbing Solutions. *ChemSusChem* **2017**, *10*, 1085−1093.

(13) Guan, C.; Pan, Y.; Ang, E. P. L.; Hu, J.; Yao, C.; Huang, M.-H.; Li, H.; Lai, Z.; Huang, K.-W. Conversion of CO_2 from air into formate using amines and phosphorus-nitrogen PN^3P-Ru(II) pincer complexes. *Green Chem* **2018**, *20*, 4201−4205.

(14) Afreen, G.; Bansode, A.; Wada, K.; Hirano, M.; Matsuda, H.; Urakawa, A. Liquid−Liquid−Gas Triphasic Hydrogenation of Bicarbonate to Formate in a Continuous Flow Tubular Reactor. *Adv. Synth. Catal* **2024**, *366*, 982−989.

(15) Roth, T. F. H.; Häusler, M.; Vogt, D.; Seidensticker, T. Advancing the aqueous biphasic hydroformylation of oleochemicals in the loop: Continuous reaction and separation using a jet-loop reactor concept. *Catal. Today* **2024**, *439*, 114803.

(16) Herrmann, N.; Bianga, J.; Palten, M.; Riemer, T.; Vogt, D.; Dreimann, J. M.; Seidensticker, T. Improving Aqueous Biphasic Hydroformylation of Unsaturated Oleochemicals Using a Jet-Loop-Reactor. *Eur. J. Lipid Sci. Technol* **2020**, *122*, 1900166.

(17) Künnemann, K. U.; Schurm, L.; Lange, D.; Seidensticker, A.; Tilloy, S.; Monflier, E.; Vogt, D.; Dreimann, J. M. Continuous hydroformylation of 1-decene in an aqueous biphasic system enabled by methylated cyclodextrins. *Green Chem* **2020**, *22*, 3809−3819.

(18) Van't Riet, K. Review of Measuring Methods and Results in Nonviscous Gas−Liquid Mass Transfer in Stirred Vessels. *Ind. Eng. Chem. Process Des. Dev* **1979**, *18*, 357−364.

(19) Schrimpf, M.; Graefe, P. A.; Holl, A.; Vorholt, A. J.; Leitner, W. Effect of Liquid−Liquid Interfacial Area on Effect of Liquid−Liquid Interfacial Area on Biphasic Catalysis Exemplified by Hydroformylation. *ACS Catal* **2022**, *12*, 7850−7861.

(20) Martín, A. J.; Mitchell, S.; Mondelli, C.; Jaydev, S.; Pérez-Ramíre, J. Unifying views on catalyst deactivation. *Nat. Catal* **2022**, *5*, 854−866.

(21) Crabtree, R. H. Deactivation in Homogeneous Transition Metal Catalysis: Causes, Avoidance, and Cure. *Chem. Rev* **2015**, *115*, 127−150.

(22) van Leeuwen, P. W. N. M. Decomposition pathways of homogeneous catalysts. *Appl. Catal., A* **2001**, *212*, 61−81.

(23) Wachsen, O.; Himmler, K.; Cornils, B. Aqueous biphasic catalysis: Where the reaction takes place. *Catal. Today* **1998**, *42*, 373−379.

(24) Widianto, A. Y.; Aubin, J.; Xuereb, C.; Poux, M. Gas−liquid−liquid reactions: Contacting mechanisms and effective process technologies. *Catal. Today* **2020**, *346*, 46−57.

https://doi.org/10.1021/jacsau.6c00388
JACS Au 2026, 6, 3386−3393